Decadal-mean impact of including ocean surface currents in bulk formulas on surface air-sea fluxes and ocean general circulation

Yang Wu[1], Xiaoming Zhai[2] and Zhaomin Wang[1]

[1]College of Oceanography, Hohai University, Nanjing, China

[2]Centre for Ocean and Atmospheric Sciences, School of Environmental Sciences, University of East Anglia, Norwich, UK

Correspondence to: Xiaoming Zhai (Xiaoming.Zhai@uea.ac.uk) and Zhaomin Wang (Zhaomin.Wang@hhu.edu.cn).

Abstract

The decadal-mean impact of including ocean surface currents in the bulk formulas on surface air-sea fluxes and the ocean general circulation is investigated for the first time using a global eddy-permitting coupled ocean-sea ice model. Although including ocean surface currents in air-sea flux calculations only weakens the surface wind stress by a few percent, it significantly reduces wind power input to both geostrophic and ageostrophic motions, and damps the eddy and mean kinetic energy throughout the water column. Furthermore, the strengths of the horizontal gyre circulations and the Atlantic Meridional Overturning Circulation are found to decrease considerably (by 10-15% and ~13%, respectively). As a result of the weakened ocean general circulation, the maximum northward global ocean heat transport decreases by ~0.2 PW, resulting in a lower sea surface temperature and reduced surface heat loss in the northern North Atlantic. Additional sensitivity model experiments further demonstrate that it is including ocean surface currents in the wind stress calculation that dominates this decadal impact, with including ocean surface currents in the turbulent heat flux calculations making only a minor contribution. Our results highlight the importance of properly accounting for ocean surface currents in surface air-sea fluxes in modelling the ocean circulation and climate.

1. Introduction

Air-sea momentum and heat transfer plays a fundamental role in driving the circulations of both the oceans and atmosphere (e.g., Gill 1982; Siedler et al. 2013). The surface momentum and turbulent heat fluxes are typically calculated based on the bulk formulas (e.g., Dawe and Thompson 2006):

$$\boldsymbol{\tau} = \rho_a c_d |\mathbf{U}_{10} - \mathbf{u}|(\mathbf{U}_{10} - \mathbf{u}) \quad (1)$$

$$Q_s = \rho_a c_{pa} C_h |\mathbf{U}_{10} - \mathbf{u}|(T_a - T_0) \quad (2)$$

$$Q_L = \rho_a L_e C_e |\mathbf{U}_{10} - \mathbf{u}|(q_a - q_s), \quad (3)$$

where ρ_a and T_a are air density and temperature at the sea surface, respectively; $\mathbf{U}_{10}$ is the 10-m wind velocity; $\mathbf{u}$ is the ocean surface velocity; c_d, C_h and C_e are stability-dependent bulk transfer coefficients for wind stress ($\boldsymbol{\tau}$), sensible heat (Q_s) and latent heat (Q_L), respectively; c_{pa} is the specific heat of air; L_e is the latent heat of evaporation; T_0 is the sea surface temperature (SST); q_a is the specific humidity; and q_s is the saturated specific humidity at SST. Eqs. (1)-(3) state that air-sea momentum and turbulent heat fluxes depend on the relative motion between the 10-m wind and the ocean surface current. Since the speed of the ocean surface currents is at least an order of magnitude smaller than that of the 10-m wind over most of the ocean, ocean surface currents are often assumed to have a negligible effect on air-sea fluxes and Eqs. (1)-(3) can be approximated by setting $\mathbf{u} = 0$, i.e.,

$$\boldsymbol{\tau} = \rho_a c_d |\mathbf{U}_{10}|\mathbf{U}_{10} \quad (4)$$

$$Q_s = \rho_a c_{pa} C_h |\mathbf{U}_{10}|(T_a - T_0) \quad (5)$$

$$Q_L = \rho_a L_e C_e |\mathbf{U}_{10}|(q_a - q_s). \quad (6)$$

A number of recent studies, however, have shown that not accounting for ocean surface currents in the wind stress calculation can lead to a positive bias in the estimate of wind power input to the ocean (e.g., Duhaut and Straub 2006; Dawe and Thompson 2006; Zhai and Greatbatch 2007; Hughes and Wilson 2008; Scott and Xu 2009; Zhai et al. 2012). For example, Zhai and Greatbatch (2007) found that including ocean surface currents in the stress calculation reduced the total wind work in a model of the northwest Atlantic Ocean by about 20%. A similar percentage of reduction in wind power input to the near-inertial motions was reported by Rath et al. (2013) when they included ocean surface currents in the calculation of wind stress in a realistic eddy-resolving Southern Ocean model. Although accounting for the relative motion between the atmosphere and the surface ocean only leads to relatively small changes in the magnitude of the time-mean wind stress, e.g., ~2% when averaged over the North Pacific (Dawe and Thompson 2006), it systematically damps surface ocean currents, particularly the energetic ocean eddy field (e.g., Zhai and Greatbatch 2007; Eden and Dietze 2009; Munday and Zhai 2015; Xu et al. 2016; so-called "relative wind stress effect"). For example, Zhai and Greatbatch (2007) reported a ~10% decrease in the eddy kinetic energy (EKE) in their northwest Atlantic model when ocean surface currents were included in the stress calculation. Eden and Dietze (2009) found a similar amount of reduction in EKE at high latitudes in an eddy-resolving model of the North Atlantic, but a much greater reduction (~50%) in the tropical Atlantic. Including ocean surface currents in the wind stress calculation has also been found to reduce the strength of equatorial upwelling to a more realistic level, thereby improving model simulations of the tropical oceans (e.g., Pacanowski 1987; Luo et al. 2005; Dawe and Thompson 2006; Eden and Dietze 2009).

In comparison, there have been fewer studies on the effect of ocean surface currents on air-sea turbulent heat fluxes (see Dawe and Thompson 2006 for an exception). Since ocean surface currents tend to, on average, move in directions similar to the surface winds, accounting for the relative motion between the atmosphere and the surface ocean is expected to reduce the magnitude of surface turbulent heat fluxes. In a 1/5^{o} regional model of the North Pacific, Dawe and Thompson (2006) found that including ocean surface currents in the bulk formulas indeed reduces surface latent and sensible heat fluxes by about 10% in the Kuroshio region, although the basin-averaged heat flux reduction is of much smaller magnitude, i.e., only 1-2%. Interestingly, the opposite effect was found in the tropical Pacific where latent and sensible heat fluxes increase due to a warming of SST as a result of changes in ocean circulation. Results from Dawe and Thompson (2006) suggested that changes in surface turbulent heat fluxes brought about by accounting for ocean surface currents in the bulk formulas may result from not only the direct effect of including ocean surface currents in the heat flux calculation but also the indirect effect of including ocean surface currents in the wind stress calculation, the latter of which influences SST and hence surface heat fluxes via ocean circulation changes. However, the relative importance of the direct and indirect effects is unknown.

So far, the focus of previous studies on this topic has been primarily on the reduction of wind power input to the ocean circulation and damping of EKE, and, to some extent, on equatorial upwelling. There have been few studies reporting the impact of accounting for ocean surface currents in air-sea flux calculations on the ocean general circulation and heat transport. Furthermore, previous investigations often rely on regional ocean model simulations of a short duration, e.g., 2 years in Dawe and Thompson (2006) and Zhai and Greatbatch (2007) and 5 years in Eden and Dietze (2009). As such, these studies are unable to address the longer term (e.g., decadal) impact on the global ocean. Here we investigate for the first time the decadal-mean impact of accounting for ocean surface currents in the bulk formulas on air-sea exchanges and the ocean general circulation using a global eddy-permitting coupled ocean-sea ice model. We also conduct additional sensitivity experiments to assess the relative importance of including ocean surface currents in the wind stress and heat flux calculations in causing this impact on decadal time scale.

The paper is organized as follows. Section 2 provides a brief model description and experiment design. Section 3 describes and discusses the effect of accounting for ocean surface currents in the bulk formulas on air-sea momentum and turbulent heat fluxes and its impact on the ocean general circulation, ocean energetics and heat transport. Section 4 concludes with a brief summary of our results.

2. Model experiments

The numerical model used in this study is the same as that in Wu et al. (2016), i.e., the MIT general circulation model (MITgcm; Marshall et al. 1997a, b) in the state estimate configuration of Estimating the Circulation and Climate of the Ocean, phase 2 (ECCO2), and the following text is derived from there with some minor modifications.

This model employs a cube-sphere grid configuration that avoids polar singularities and permits relatively even grid spacing throughout the model domain (Adcroft et al. 2004). The mean horizontal grid spacing of the model is 18 km, i.e., eddy-permitting, and the model has 50 uneven vertical levels with their thickness increasing from 10 m near the surface to 450 m at the bottom. The sub-grid scale vertical mixing processes are parameterized using the K-Profile Parameterization (Large et al. 1994), and no explicit eddy parameterization schemes are used in the model. The ocean model is coupled to the MITgcm sea ice model and is run with optimized parameters that are obtained to reduce model-data misfit via the Green Function approach (Menemenlis et al. 2005, 2008). The coupled model is forced by 6-hourly atmospheric data taken from the Japanese 55-year Reanalysis (JRA-55) dataset for the period of 1979-2012 (Kobayashi et al. 2015), including 6-hourly downward longwave radiation, downward shortwave radiation, 2-m humidity, 2-m air temperature, precipitation, and 10-m wind velocity. There is some uncertainty in parameters used in the bulk formula, e.g., the drag coefficient, but this uncertainty is unlikely to qualitatively changes the results shown in this paper. The model is initialized from a blend of the Polar Hydrographic Climatology, the World Ocean Circulation Experiment Global Hydrographic Climatology and a spin-up run of ECCO2 (Menemenlis et al. 2008).

To investigate the impact of including ocean surface currents in the bulk formulas on surface air-sea fluxes and the ocean general circulation, we conduct three model experiments with the only difference between them being whether ocean surface currents are included in the bulk formulas. In experiment CONTROL, ocean surface currents are included in the calculations of both air-sea momentum and turbulent heat fluxes, i.e., Eqs. (1)-(3) are used in CONTROL. In experiment NONE, ocean surface currents are excluded from air-sea flux calculations, i.e., Eqs. (4)-(6) are used in NONE. In the third experiment, HEAT, ocean surface currents are included in the turbulent heat flux calculations, but not in the wind stress calculation, i.e. Eqs. (2)-(4) are used in HEAT. Differences between CONTROL and HEAT (and also between HEAT and NONE) are then used to assess the relative importance of including ocean surface currents in air-sea momentum and heat flux calculations. All three experiments are initialized with the same blended climatology and integrated for 34 years from 1979 to 2012. Except for the wind power input calculations where instantaneous outputs every 3 days are used, monthly-averaged model outputs from the last 10 years[1] of the three experiments at 18 km resolution are analyzed for this study.

3. Results

a. Air-sea fluxes

1) MOMENTUM FLUX

Including ocean surface currents in the bulk formulas leads to a slight but wide-spread weakening of the mean surface wind stress (Fig. 1a). This weakening in surface wind stress is more pronounced in regions where ocean surface currents are relatively strong. For example, the strength of the mean wind stress averaged over the Kuroshio Extension region (165^{o}E-120^{o}W, 30^{o}N-60^{o}N) is about 6% weaker in CONTROL than

[1]Using model outputs from only the last 5 years makes little differences to the results shown in this paper.

in NONE, in agreement with the 5-10% difference reported by Dawe and Thompson (2006). Similar percentage decreases are also found in the Gulf Stream region, the tropics, and the Southern Ocean when ocean surface currents are included in the bulk formulas. When averaged over the global ocean, the mean wind stress in CONTROL is about ~4% weaker than those in NONE and HEAT. The close resemblance between Figs. 1a and 1b in terms of both magnitude and spatial pattern demonstrates that the difference in the mean wind stress between CONTROL and NONE is due primarily to the effect of including ocean surface currents in the calculation of surface wind stress, as one would expect. The wide-spread weakening of the mean wind stress shown in Fig. 1b confirms that ocean surface currents are indeed generally orientated in directions similar to the surface winds. One exception is the North Pacific Counter Current which flows eastward against the prevailing trade winds.

This slight weakening of the mean wind stress owing to the presence of ocean surface currents in the wind stress calculation leads to a general reduction in the magnitude of the wind stress curl, most noticeable in the Southern Ocean, the equatorial current system and the high northern latitudes (Fig. 1d). Large differences in the mean wind stress curl between CONTROL and NONE are found in regions of ocean fronts and jets, often characterized by dipole patterns. For example, including ocean surface currents in the bulk formulas results in negative (positive) wind stress curl to the north (south) of the Sub-Antarctic Front. This is because the reduction in the strength of the mean wind stress after taking into account the relative motion between the atmosphere and the surface ocean tends to be most significant along the jet axis, which then creates anomalous horizontal wind stress shear of opposite sign on either side of the jets. Similar dipole patterns are also found in the Gulf Stream region and the tropical oceans.

2) HEAT FLUX

Figure 2 shows the time-mean net surface heat flux averaged over the last decade in CONTROL and the differences between the three experiments. Although the overall patterns of the mean surface heat fluxes in all three experiments are very similar, including ocean surface currents in air-sea flux calculations leads to a significant reduction in surface heat loss in the subpolar North Atlantic as well as anomalous heat gain (loss) equatorward (poleward) of the western boundary currents (Fig. 2b). Heat loss averaged over the subpolar North Atlantic (70^{o}W-0^{o}, 40^{o}N-80^{o}N) decreases by ~14.4% from -46 W m^{-2} in NONE to -39 W m^{-2} in CONTROL. Interestingly, comparison between Fig. 2b and Fig. 2c makes it clear that the differences in surface heat flux between CONTROL and NONE are not a direct effect of including ocean surface currents in the turbulent heat flux calculations, but mainly an indirect effect of including ocean surface currents in the wind stress calculation via ocean circulation differences between the two experiments.

Differences in surface heat flux between CONTROL and NONE are closely linked to their SST differences (Fig. 3). The pronounced heat flux differences in the subpolar North Atlantic and the western boundary current regions are in opposite phase to the SST differences in those regions, demonstrating that it is changes of SST that lead to changes in surface heat flux there, not vice versa (see Eqs. 2 and 3). Comparisons between the three experiments (Figs. 3b-d) further confirm that the SST differences between CONTROL and NONE, especially those in extratropics, are mainly a result of ocean circulation differences induced by different wind stress calculations, i.e., Eq. (1) vs. Eq. (4), although including ocean surface currents in the turbulent heat flux calculations makes an important contribution in the tropical oceans. It will be shown later that the SST differences between CONTROL and NONE in the subpolar North Atlantic are mostly associated with differences in the strength of the Atlantic Meridional Overturning Circulation (AMOC) while those in the western boundary current regions associated with differences in the horizontal gyre circulations.

The results above demonstrate that, on decadal time scale, the indirect effect of including ocean surface currents in the wind stress calculation dominates the differences in air-sea heat fluxes and the SST over the direct effect of including ocean surface currents in the heat flux calculation. It is instructive to examine whether this also holds on much shorter time scales. Figure 4 shows the differences in surface heat flux and the SST averaged over the first model day between the three experiments. Although these differences are still very small in magnitude, it is clear that the immediate response of surface heat flux is almost entirely explained by the direct effect of including ocean surface currents in the heat flux calculations. Since ocean surface currents, generally speaking, are orientated in directions similar to the surface winds, $|\mathbf{U}_{10} - \mathbf{u}|$ is typically smaller than $|\mathbf{U}_{10}|$[2]. Including ocean surface currents in the heat flux calculations therefore reduces the surface turbulent heat loss and increase the net heat gain over most of the global ocean (Figs. 4a and 4c). One exception is the

[2] This is not necessarily true for ocean eddies.

equatorial counter current region where $|\mathbf{U}_{10} - \mathbf{u}|$ is actually greater than $|\mathbf{U}_{10}|$. Due to the dominance of the direct heat flux effect, differences in SST averaged over the first model day between the three experiments are generally in phase with differences in surface heat flux, i.e., reduced surface heat loss resulting in warmer SST. However, the dominance of this direct effect is rather short-lived. When averaged over the first model month, the indirect effect of different wind stress calculations already starts to play a more important role in determining the surface heat flux and SST differences between these experiments (not shown).

b. Wind power input

The wind power input, *P*, is calculated here using $P = \overline{\boldsymbol{\tau} \cdot \mathbf{u}}$, where the overbar denotes a 10-year time average. The spatial patterns of *P* in all three experiments are similar to those in previous studies (e.g. Huang et al. 2006; von Storch et al. 2012), with most of the wind power input concentrated in the Southern Ocean (not shown). Integrated globally, *P* in NONE is ~3.41 TW (1 TW = 10^{12} W), of which 1.27 TW is supplied by the time-mean wind stress ($\overline{\boldsymbol{\tau}} \cdot \overline{\mathbf{u}}$) and 2.14 TW by the time-varying wind stress ($\overline{\boldsymbol{\tau}' \cdot \mathbf{u}'}$). These values are lower than, but comparable to, $\overline{\boldsymbol{\tau}} \cdot \overline{\mathbf{u}} = 1.85$ TW and $\overline{\boldsymbol{\tau}' \cdot \mathbf{u}'} = 2.19$ TW that were found by von Storch et al. (2012) in their 1/10° global STORM/NCEP simulation where ocean surface currents were not accounted for in the wind stress calculation. In comparison, *P* in CONTROL is only ~2.55 TW, of which 1.14 TW is supplied by $\overline{\boldsymbol{\tau}} \cdot \overline{\mathbf{u}}$ and 1.41 TW by $\overline{\boldsymbol{\tau}' \cdot \mathbf{u}'}$, representing a 25.2%, 10.2% and 34.1% reduction in *P*, $\overline{\boldsymbol{\tau}} \cdot \overline{\mathbf{u}}$ and $\overline{\boldsymbol{\tau}' \cdot \mathbf{u}'}$ respectively from NONE (see Table 1). Figure 5a shows that the reduction in *P* is most significant in the Southern Ocean, the tropics, and mid and high northern latitudes.

Given that including ocean surface currents in the stress calculation only leads to a slight weakening of the surface wind stress (Fig. 1), the percentage reduction of P seems surprisingly large. This large effect of the relative wind stress on P can be understood by simple scaling arguments. Following Duhaut and Straub (2006), we decompose $\mathbf{u}$ into the sluggish large-scale $\mathbf{u_{basin}}$ and more energetic mesoscale $\mathbf{u_{eddy}}$, with $|\mathbf{u_{basin}}| \ll |\mathbf{u_{eddy}}|$. In the absence of the relative wind effect, $\boldsymbol{\tau}$ is expected to project onto $\mathbf{u_{basin}}$, not $\mathbf{u_{eddy}}$, such that $\boldsymbol{\tau} \cdot \mathbf{u} \approx \boldsymbol{\tau} \cdot \mathbf{u_{basin}}$. It can then be shown after some simple algebra that the percentage reduction of P scales as $\frac{|\mathbf{u}|^2}{|\mathbf{U_{10}}||\mathbf{u_{basin}}|} \approx \frac{|\mathbf{u_{eddy}}|^2}{|\mathbf{U_{10}}||\mathbf{u_{basin}}|}$, which is roughly 20% if one plugs in $|\mathbf{U_{10}}| \sim 10 \text{ m s}^{-1}$, $|\mathbf{u_{eddy}}| \sim 0.2 \text{ m s}^{-1}$ and $|\mathbf{u_{basin}}| \sim 0.02 \text{ m s}^{-1}$.

It is instructive to separate wind power input that goes into surface geostrophic motions ($P_g = \overline{\boldsymbol{\tau} \cdot \mathbf{u_g}}$) from that goes into surface ageostrophic motions ($P_a = \overline{\boldsymbol{\tau} \cdot \mathbf{u_a}}$). Including ocean surface currents in the bulk formulas reduces the globally-integrated P_g and P_a by about 0.13 TW (15%) and 0.73 TW (29%), respectively. Most of the small-scale structures seen in Fig. 5a are due to differences in P_g between CONTROL and NONE (Fig. 5c), while P_a shows a much more spatially uniform reduction (Fig. 5b). The significant reduction in P_a is likely to lead to reduced vertical mixing in the upper ocean, since the majority of P_a is dissipated within the upper few tens of meters, contributing to the deepening of the surface mixed layer and cooling of the SST (e.g. Zhai et al. 2009). It is worth pointing out that the net values of P_g and P_a found in this study compare favorably with a number of previous studies. The P_g=0.73 TW in

CONTROL is close to the 0.76 TW estimated by Hughes and Wilson (2008) who accounted for the relative wind stress effect, while the P_g=0.86 TW in NONE agrees well with the 0.88 TW estimated by Wunsch (1998) who did not account for the relative wind stress effect. For P_a, its net value is ~2.55 TW in NONE, comparable to the 2.4 TW estimated by Wang and Huang (2004) based on classical Ekman dynamics.

Figure 6 shows that wind power input to the ocean circulation by the time-varying wind stress in CONTROL is dominated by $\overline{\boldsymbol{\tau}' \cdot \mathbf{u_a}'}$, with $\overline{\boldsymbol{\tau}' \cdot \mathbf{u_g}'}$ actually making negative contributions over many areas at mid and high latitudes. Negative values of $\overline{\boldsymbol{\tau}' \cdot \mathbf{u_g}'}$ in regions of strong eddy activities is owing to the relative wind stress damping effect which is proportional to the magnitude of ocean surface kinetic energy (Duhaut and Straub 2006; Xu et al. 2016). In contrast, $\overline{\boldsymbol{\tau}' \cdot \mathbf{u_a}'}$ is positive everywhere, since the time-varying ageostrophic ocean currents (e.g., Ekman currents) are generally orientated in directions similar to the time-varying wind stress. Including ocean surface currents in the wind stress calculation leads to a reduction of $\overline{\boldsymbol{\tau}' \cdot \mathbf{u}'}$ by 0.73 TW, of which 0.68 TW is owing to reduction in $\overline{\boldsymbol{\tau}' \cdot \mathbf{u_a}'}$ and only 0.05 TW owing to reduction in $\overline{\boldsymbol{\tau}' \cdot \mathbf{u_g}'}$. Comparisons between the three experiments show that differences in wind power input between CONTROL and NONE is due to the relative wind stress effect (see Table 1).

c. Ocean kinetic energy

Consistent with previous studies, including ocean surface currents in air-sea flux calculations leads to a widespread reduction in surface EKE (Figs. 7a and b). Here EKE is defined as $\overline{(u'^2 + v'^2)}/2$, where u and v are zonal and meridional velocities. The reduction is most pronounced in the tropical oceans, but also significant in the western boundary current regions and the Southern Ocean. Integrated globally, EKE in CONTROL and NONE are 0.94 EJ and 1.29 EJ respectively, representing a reduction of ~27%. In comparison, the globally-integrated EKE in HEAT is about 1.26 EJ, almost identical to that in NONE, confirming that the reduction of EKE is due almost entirely to the relative wind stress damping effect. The small-scale structures of alternating signs in Fig. 7c are associated with mesoscale eddies, and they largely cancel each other when integrated over the model domain.

There have been few studies reporting the vertical structure of EKE damping by the relative wind stress. Here we find that the reduction in EKE is most significant at the sea surface, which then decays with depth over a distance of 600-1000 m (Figs. 8a-c). The surface EKE integrated over the Southern Ocean, the tropics, and the global ocean in CONTROL are 18.2%, 44.2% and 32.6% less than those in NONE, respectively. These percentage decreases are comparable to the 18% reduction of surface EKE found by Munday and Zhai (2015) in an idealized Southern Ocean model and the 50% reduction of surface EKE found by Eden and Dietze (2009) in the tropical Atlantic when ocean surface currents are included in the wind stress calculation. Interestingly, although the magnitude of EKE reduction is found to decrease with depth, the percentage reduction of the globally-averaged EKE remains at roughly 20-30% below the upper 400 m (Fig. 8d).

Including ocean surface currents in the bulk formulas also leads to a reduction in the surface mean kinetic energy (MKE) over most of the ocean, most noticeably in the tropics and, to a lesser extent, in the western boundary current regions (Fig. 7d). For example, MKE integrated over the global ocean decreases by about 12.5% from 0.8 EJ in NONE to 0.7 EJ in CONTROL, with nearly half of the decrease being in the tropics. In contrast to the deep-reaching structure of EKE reduction, the reduction of MKE is confined much closer to the surface, i.e., within the top 150 m (Figs. 8e-g), although the percentage decrease remains roughly 10% below the upper 500 m (Fig. 8h). It is worth pointing out that differences in surface MKE shown in Fig. 7d are due mostly to differences in the geostrophic, rather than Ekman, part of the mean flow between the two experiments. Only very small differences are found in MKE averaged over the Southern Ocean between the three experiments (Fig. 8f), an interesting feature that we will discuss further in the next section. Again, it is including ocean surface currents in the wind stress calculation that is responsible for the difference in MKE between CONTROL and NONE (Figs. 7d-f).

d. Gyre circulation and ACC transport

Differences in the mean wind stress curl between CONTROL and NONE are likely to lead to differences in the depth-integrated meridional volume transport and hence the gyre circulations. However, to our knowledge, the effect on gyre circulations has not been investigated in detail before. Figure 9 shows that including ocean surface currents in the bulk formulas reduces the strength of the simulated gyre circulations almost everywhere. For example, the mean strength of the North Atlantic subtropical gyre decreases by about 10.3% from 97.3 Sv in NONE to 87.3 Sv in CONTROL, and that of the North Atlantic subpolar gyre decreases by about 16.4% from 63.3 Sv in NONE to 52.9 Sv in CONTROL, becoming more comparable with the observed value of 48.8 Sv (e.g. Reynaud et al. 1995). Similar reductions in the strength of the gyre circulations are also found in the South Atlantic and the Pacific (see Table 2). The associated weakening and meridional shift of the western boundary currents appear to be largely responsible for the differences in SST and surface heat flux found between CONTROL and NONE in these regions (Figs. 2 and 3). In the tropical Pacific, including ocean surface currents results in a set of positive and negative zonal bands owing to the reduction of the strength of the North Equatorial Current and the South Equatorial Current (see also Dawe and Thompson 2006). Comparisons between the three experiments show that differences in the strength of the horizontal gyre circulations are due primarily to the effect of including ocean surface currents in the wind stress calculation.

On the other hand, the Antarctic Circumpolar Current (ACC) transport at Drake Passage in CONTROL remains very similar to those in NONE and HEAT (see Table 2 and Fig. 8f). The mean ACC transports averaged over the last decade in CONTROL and NONE are both about 92 Sv, despite of the ~9% decrease in the mean wind stress and ~28% reduction in EKE in the Southern Ocean in CONTROL. Furthermore, there is virtually no difference in isopycnal slopes in the Southern Ocean between the three experiments (not shown). This insensitivity of ACC transport to surface wind forcing appears to be consistent with the findings of a number of recent studies (e.g. Straub 1993; Meredith and Hogg 2006; Wang et al. 2011; Munday et al. 2013; Munday and Zhai 2017) who found the ACC is in an eddy-saturated state where changes of surface wind forcing is at least partially compensated by changes of the eddy field, rendering little changes in isopycnal slopes and the equilibrium ACC transport. Similar insensitivity of ACC transport to different wind stress bulk formulas was also found by Munday and Zhai (2015) in an idealized eddying Southern Ocean channel model.

e. Deep convection and AMOC

We now analyze the effect of including ocean surface currents in the bulk formulas on the mixed layer depth (MLD) and the intensity of deep convection at high latitudes. The MLD in the ECCO2 state estimate is defined as the depth at which the density differs from that at the ocean surface by an amount that is equivalent to a temperature difference of 0.8^{o}C, an optimal value estimated by Kara et al. (2000) to best fit two observational datasets.

Figure 10 shows the spatial distributions of the late winter MLD in CONTROL averaged over the last decade and the differences between the three experiments. Deep winter surface mixed layers are found in the western boundary current regions, the Southern Ocean, the subpolar North Atlantic and the Nordic Seas in all three experiments. When ocean surface currents are included in the bulk formulas, the winter MLD decreases considerably at mid and high latitudes, particularly in the subpolar North Atlantic and the Southern Ocean (Fig. 10b). For example, the March-mean MLDs averaged in the Labrador Sea in CONTROL and NONE are 2750 m and 3450 m respectively, representing a ~20% difference. Interestingly, it is the effect of including ocean surface currents in the wind stress calculation, rather than turbulent heat flux calculations, that explains most of the differences in MLD between CONTROL and

NONE (Figs. 10b-d). As Fig. 1d shows, including ocean surface currents in the wind stress calculation weakens the cyclonic wind stress curl in the subpolar North Atlantic in CONTROL. For example, the March-mean cyclonic wind stress curl averaged in the Labrador Sea in CONTROL is about 20% weaker than that in NONE. The weakened cyclonic wind stress curl in CONTROL reduces the strength of Ekman upwelling and results in less doming of the density surfaces and a weaker cyclonic circulation in the subpolar North Atlantic than in NONE (Fig. 9). We argue that this reduced preconditioning effect then makes it harder for surface heat loss to overcome stratification and trigger deep-reaching convection in CONTROL (Marshall and Schott 1999).

The differences in the intensity of deep convection in the northern North Atlantic between the experiments are expected to have an impact on the strength of the AMOC (e.g. Eden and Willebrand 2001; Zhai et al. 2011; Zhai et al. 2014; Wu et al. 2016). The AMOC is calculated here in the same way as Wu et al. (2016) by zonally integrating the meridional velocity across the Atlantic basin from its western boundary (x_W) to eastern boundary (x_E) and from the ocean bottom at $z = -h$ upward: $\psi(y,z,t) = \int_{-h}^{z}\int_{x_W(y,z)}^{x_E(y,z)} v(x,y,z,t)dxdz$. Figure 11 shows that including ocean surface currents in the bulk formulas leads to a coherent reduction in the strength of AMOC at all latitudes. The maximum strength of the AMOC decreases by about 12.6% from 20.6 Sv in NONE to 18.0 Sv in CONTROL. There is also a slight reduction (~0.76 Sv) in the strength of the overturning cell in the abyssal ocean. Comparisons between the three experiments further demonstrate that the reduction in the strength of the AMOC in CONTROL is mainly a result of including ocean surface currents in the wind stress calculation, consistent with the differences in the intensity of deep convection shown in Fig. 10.

f. Meridional heat transport

Results from previous sections show that including ocean surface currents in air-sea flux calculations can lead to considerable changes in the strength of the horizontal gyre circulations and the AMOC. We now investigate the impact of these ocean circulation changes on the meridional heat transport. The overall structures of the meridional ocean heat transport in the three experiments are similar to each other and comparable to those inferred from observations (e.g., Trenberth and Caron 2001; Ganachaud and Wunsch 2003), with the wind-driven gyre circulations primarily responsible for the poleward heat transport in the Pacific Ocean and Indian Ocean and the AMOC dominating the northward heat transport in the Atlantic Ocean (Fig. 12).

When ocean surface currents are included in the bulk formulas, the magnitude of meridional heat transport decreases in all the ocean basins. In the Atlantic Ocean, the northward heat transport in CONTROL is weaker than that in NONE at all latitudes, with the peak northward heat transport decreasing by about 14.8% from 1.08 PW (1 PW = 10^{15} W) in NONE to 0.92 PW in CONTROL (Fig. 12b). The reduced northward heat transport in the Atlantic, mainly as a result of the weakened AMOC, results in a colder SST in the northern North Atlantic in CONTROL (Fig. 3), which, in turn, reduces the surface heat loss there (Fig. 2). In the Pacific Ocean, the maximum northward heat transport decreases by about 15.5% from 0.58 PW in NONE to 0.49 PW in CONTROL. Globally, including ocean surface currents in the bulk formulas reduces the maximum northward heat transport in the North Hemisphere by ~0.2 PW from 1.7 PW in NONE to 1.5 PW in CONTROL, that is, a 12% decrease. In comparison, the reduction of the southward heat transport in the Southern Hemisphere is much less owing to cancellation between simultaneous reductions of the northward heat transport in the South Atlantic and southward heat transport in the Indo-Pacific Oceans. Again, it is including ocean surface currents in the wind stress calculation that is responsible for the reduction in the meridional ocean heat transport shown in Fig. 12.

4. Summary

In this study we have investigated for the first time the decadal-mean impact of including ocean surface currents in the bulk formulas on surface air-sea fluxes and the ocean general circulation using a global coupled ocean-sea ice model at eddy-permitting resolution. By comparing model simulations that include, partially include, and exclude ocean surface currents in air-sea flux calculations, we find

- The decadal-mean impact on surface air-sea fluxes and ocean circulation is dominated by the effect of including ocean surface currents in the wind stress calculation, with the effect of including ocean surface currents in the heat flux calculations making only a minor contribution.
- Including ocean surface currents in the bulk formulas leads to a general reduction in the magnitude of surface wind stress (and also its curl) and a significant reduction in surface heat loss in the northern North Atlantic. This reduction in surface heat loss is associated with the colder SST there as a result of ocean circulation changes.
- Including ocean surface currents in the bulk formulas reduces wind power input to

surface geostrophic motions by about 0.13 TW and that to surface ageostrophic motions by about 0.73 TW.

- Consistent with previous studies, including ocean surface currents in the bulk formulas damp both the EKE and MKE in the ocean considerably. The globally integrated EKE and MKE decrease by about 27% and 12.5%, respectively. Although this relative wind stress damping effect is surface intensified, it extends throughout the water column.
- Including ocean surface currents in the bulk formulas leads to a reduction in the strength of the horizontal gyre circulations by 10-15%. In contrast, the ACC transport remains largely unchanged despite of considerable changes of the wind stress and EKE in the Southern Ocean.
- Including ocean surface currents in the bulk formulas reduces the intensity of deep convection in the northern North Atlantic, which, in turn, weakens the AMOC by about 12.6%.
- The weakened horizontal gyre circulations and the AMOC reduce the magnitude of the meridional heat transport in all ocean basins. The maximum northward global ocean heat transport decreases by about 12% from 1.7 PW to 1.5 PW.

Results from our study show that accounting for the relative motion between the atmosphere and the surface ocean in air-sea flux calculations, particularly in the wind stress calculation, can lead to a significant reduction in the strength of the simulated ocean general circulation and meridional heat transport on decadal time scale. Ocean models that do not account for this relative motion are therefore likely to be forced too strongly and miss an important ocean energy sink. Recent studies (Zhai et al. 2012) suggest that the relative wind stress damping effect is strongly enhanced by wind variability associated with synoptic weather systems. This implies that a significant fraction of the differences between CONTROL and NONE shown in this study may be explained by the synoptic wind variability resolved by the JRA-55 reanalysis product. Efforts are currently underway to quantify the role played by synoptic weather systems in determining the impact of different bulk formulas on the ocean general circulation.

There are several limitations associated with our study. For example, the model we use is only of eddy-permitting resolution, so the relative wind stress damping effect is likely to be underestimated since the damping effect is proportional to the magnitude of surface kinetic energy. On the other hand, recent studies using coupled models (Renault et al. 2016; Abel et al. 2017) suggest that the near-surface winds may be somewhat enhanced due to the ocean current feedback, which may partly counteract damping by the relative wind stress and therefore partly re-energize the ocean. This so-called re-energization effect is not included in our ocean-only model experiments. Finally, although some of the results shown here may depend quantitatively on the model we use, weakening of the ocean general circulation as a result of reduced wind power input is consistent with the view that the large-scale ocean circulation is maintained by mechanical energy input into the ocean (e.g. Huang 1999; Wunsch and Ferrari 2004). The potentially significant impact of accounting for ocean surface currents in the bulk formulas on ocean circulation and climate calls for further research on this topic.

Acknowledgements. XZ acknowledges financial support provided by a Royal Society International Exchanges Award (IE131025). ZW is supported by the Major State Basic Research Development Program of China (2016YFA0601804), by the Fundamental Research Funds for the Central Universities (2017B04814), and by the China National Natural Science Foundation (NSFC) Projects (41276200, 41330425). We thank Chris Wilson and two anonymous reviewers for their helpful comments that led to an improved manuscript.

REFERENCES

Abel, R., Boning, C. W., Greatbatch, R. J., Hewitt, H. T., and Roberts, M. J., 2017: Feedback of mesoscale ocean currents on atmospheric winds in high-resolution coupled models and implications for the forcing of ocean-only models. *Ocean Sci. Discuss.*, doi:10.5194/os-2017-24.

Adcroft, A., J.-M. Campin, C. Hill, and J. Marshall, 2004: Implementation of an atmosphere-ocean general circulation model on the expanded spherical cube. *Mon. Wea. Rev.*, **132**, 2845- 2863.

Dawe, J. T., and L. Thompson, 2006: Effect of ocean surface currents on wind stress, heat flux, and wind power input to the ocean. *Geophys. Res. Lett.*, **33**(9).

Duhaut T. H. A., and D. N. Straub, 2006: Wind stress dependence on ocean surface velocity: Implications for mechanical energy input to ocean circulation. *J. Phys. Oceanogr.*, **36**, 202-211.

Eden, C., and J. Willebrand, 2001: Mechanism of interannual to decadal variability of the North Atlantic circulation. *J. Climate*, **14**, 2266-2280.

Eden, C., and H. Dietze, 2009: Effects of mesoscale eddy/wind interactions on biological new production and eddy kinetic energy. *J. Geophys. Res*., **114**, C05023.

Ganachaud, A., and C. Wunsch, 2003: Large-scale ocean heat and freshwater transports during the World Ocean Circulation Experiment. *J. Climate*, **16**, 696-705.

Gill, A. E., 1982: *Atmosphere-Ocean Dynamics*, Academic press, London, 662pp.

Huang, R. X., 1999: Mixing and energetics of the oceanic thermohaline circulation. *J.*

Phys. Oceanogr., **29**, 727-746.

Huang, R. X., W. Wang, and L. L. Liu, 2006: Decadal variability of wind-energy input to the world ocean. *Deep-Sea Res*., **19**, 31-41.

Hughes, C. W., and C. Wilson, 2008: Wind work on the geostrophic ocean circulation: An observational study on the effect of small scales in the wind stress. *J. Geophys. Res.*, **113**, doi: 10.1029/2007JC004371.

Kara, A. B., P. A. Rochford, and H. E. Hurlburt, 2000: An optimal definition for ocean mixed layer depth. *J. Geophys. Res*., **105**, 803-16,821.

Kobayashi, S., et al., 2015: The JRA-55 reanalysis: General specifications and basic characteristics. *J. Meteor. Soc. Japan*, **93**, 5-48.

Large, W. G., J. C. McWilliams, and S. C. Doney, 1994: Oceanic vertical mixing: A review and a model with a nonlocal boundary layer parameterization. *Rev. Geophys*., 32, 363-403.

Luo, J., et al., 2005: Reducing climatology bias in an ocean-atmosphere CGCM with improved coupling physics. *J. Climate*, **18**, 2344-2360.

Marshall, J., A. Adcroft, C. Hill, L. Perelman, and C. Heisey, 1997a: A finite-volume, incompressible Navier Stokes model for studies of the ocean on parallel computers. *J. Geophys. Res.*, **102**, 5753-5766.

Marshall, J., C. Hill, L. Perelman, and A. Adcroft, 1997b: Hydrostatic, quasi-hydrostatic, and nonhydrostatic ocean modeling. *J. Geophys. Res.*, **102**, 5733-5752.

Marshall J., and F. Schott, 1999: Open-ocean convection: Observations, theory, and models. *Rev. Geophys.*, **37**, 1-64.

Menemenlis, D., I. Fukumori, and T. Lee, 2005: Using Green's functions to calibrate an ocean general circulation model. *Mon. Wea. Rev.*, **133**, 1224-1240.

Menemenlis, D., J. Campin, P. Heimbach, C. Hill, T. Lee, A. Nguyen, M. Schodlock, and H. Zhang, 2008: ECCO2: High resolution global ocean and sea ice data synthesis. *Mercator Ocean Quarterly Newsletter*, **31**, 13–21.

Meredith, M. P., and A. M. Hogg, 2006: Circumpolar response of Southern Ocean eddy activity to a change in the southern annular mode. *Geophys. Res. Lett.*, **33**, L16608, doi:10.1029/2006G L 026499.

Munday, D. R., H. L. Johnson, and D. P. Marshall, 2013: Eddy saturation of equilibrated circumpolar currents. *J. Phys. Oceanogr.*, **43**, 507-532.

Munday, D. R., and X. Zhai, 2015: Sensitivity of Southern Ocean circulation to wind stress changes: Role of relative wind stress. *Ocean Modell.*, **95**, 15–24.

Munday, D. R., and X. Zhai, 2017: The impact of atmospheric storminess on the sensitivity of Southern Ocean circulation to wind stress changes. *Ocean Modell.*, **115**, 14–26.

Pacanowski, R. C., 1987: Effect of equatorial currents on surface stress. *J. Phys. Oceanogr.*, **17**, 833–838.

Rath, W., R. J. Greatbatch, and X. Zhai, 2013: Reduction of near-inertial energy through the dependence of wind stress on the ocean-surface velocity. *J. Geophys. Res.*, **118**, 2761–2773.

Renault, L., et al. 2016: Modulation of wind work by oceanic current interaction with the atmosphere. *J. Phys. Oceanogr*., **46**, 1685-1704.

Reynaud, T. H., A. J. Weaver, and R. J. Greatbatch, 1995: Summer mean circulation of the northwestern Atlantic Ocean. *J. Geophys. Res*., **100**, 779–816.

Scott, R. B., and Y. Xu, 2009: An update on the wind power input to the surface geostrophic flow of the world ocean. *Deep-Sea Res*., **56**, 295-304.

Siedler, G., S. M. Griffies, W. J. Gould, and J. Church, 2013: *Ocean Circulation and Climate: A 21st Century Perspective*, 2nd Ed, Academic Press, Amsterdam.

Straub, D. N., 1993: On the transport and angular momentum balance of channel models of the Antarctic Circumpolar Current. *J. Phys. Oceanogr.*, **23**, 776-782.

Trenberth, K. E., and J. M. Caron, 2001: Estimates of meridional atmosphere and ocean heat transports. *J. Climate*, **14**, 3433-3443.

von Storch, J., C. Eden, I. Fast, H. Haak, D. Hernndez-Deckers, E. Maier-Reimer,J. Marotzke, and D. Stammer, 2012: An estimate of Lorenz energy cycle for the world ocean based on the 1/10 STORM/NCEP simulation. *J. Phys. Oceanogr.*, **42**, 2185-2205.

Wang, W., and R. X. Huang, 2004: Wind energy input to the Ekman layer. *J. Phys. Oceanogr.*, **34**, 1276-1280.

Wang, Z., T. Kuhlbrodt, and M. P. Meredith, 2011: On the responses of the Antarctic Circumpolar Current transport to climate change in coupled climate models. *J. Geophys. Res*., **116,** C08011, doi:10.1029/2010JC006757.

Wu, Y., X. Zhai, and Z. Wang, 2016: Impact of synoptic atmospheric forcing on the mean ocean circulation. *J. Climate*, **29**, 5709-5724.

Wunsch, C., 1998: The work done by the wind on the oceanic general circulation. *J. Phys. Oceanogr.,* **28**, 2332-2340.

Wunsch, C., and R. Ferrari, 2004: Vertical mixing, energy, and the general circulation of the oceans. *Annu. Rev. Fluid Mech*., **36**, 281-314.

Xu, C., X. Zhai, and X. D. Shang, 2016: Work done by atmospheric winds on mesoscale ocean eddies. *Geophys. Res. Lett*., **43**, doi:10.1002/2016GL071275.

Zhai, X., and R. J. Greatbatch, 2007: Wind work in a model of the northwest Atlantic Ocean. *Geophys. Res. Lett.,* **34**, L04606, doi:10.1029/2006GL028907.

Zhai, X., H. L. Johnson, and D. P. Marshall, 2011: A model of Atlantic heat content and sea level change in response to thermohaline forcing. *J. Climate*, **24**, 5619-5632.

Zhai, X., H. L. Johnson, and D. P. Marshall, 2014: A simple model of the response of the Atlantic to the North Atlantic Oscillation. *J. Climate*, **27**, 4052-4069.

Zhai, X., R. J. Greatbatch, C. Eden, and T. Hibiya, 2009: On the loss of wind-induced near-inertial energy to turbulent mixing in the upper ocean. *J. Phys. Oceanogr*., **39**, 3040-3045.

Zhai, X., H. L. Johnson, D. P. Marshall, and C. Wunsch, 2012: On the wind power input to the ocean general circulation. *J. Phys. Oceanogr.*, **42**, 1357-1365.

List of Tables

TABLE 1. Wind power input (in TW) to surface geostrophic and ageostrophic motions by the time-mean and time-varying wind stresses in CONTROL, HEAT and NONE, and the differences (also in percentage) between CONTROL and NONE.

	$\overline{\tau \cdot u}$	$\overline{\tau} \cdot \overline{u}$	$\overline{\tau' \cdot u'}$	$\overline{\tau \cdot u_g}$	$\overline{\tau} \cdot \overline{u_g}$	$\overline{\tau' \cdot u'_g}$	$\overline{\tau \cdot u_a}$	$\overline{\tau} \cdot \overline{u_a}$	$\overline{\tau' \cdot u'_a}$
CONTROL	2.55	1.14	1.41	0.73	0.71	0.02	1.82	0.43	1.39
NONE	3.41	1.27	2.14	0.86	0.79	0.07	2.55	0.48	2.07
HEAT	3.42	1.25	2.17	0.84	0.78	0.06	2.58	0.47	2.11
CONTROL-NONE (%)	-0.86 (-25.2%)	-0.13 (-10.2%)	-0.73 (-34.1%)	-0.13 (-15.1%)	-0.08 (-10.1%)	-0.05 (-71.4%)	-0.73 (-28.6%)	-0.05 (-10.4%)	-0.68 (-32.9%)

TABLE 2. The mean strength (in Sv) of the main ocean gyres in CONTROL, HEAT and NONE, and percentage differences between CONTROL and NONE.

	North Atlantic Subpolar Gyre	North Atlantic Subtropical Gyre	South Atlantic Subtropical Gyre	North Pacific Subpolar Gyre	North Pacific Subtropical Gyre	South Pacific Subtropical Gyre	ACC
CONTROL	52.9	87.3	80.4	30.3	117.5	42.3	91.6
NONE	63.3	97.3	86.5	33.4	127.1	49.2	91.7
HEAT	63.2	98.3	85.4	33.2	128.3	49.8	91.5
%(CONTROL-NONE)	-16.4%	-10.3%	-7.1%	-9.3%	-7.6%	-14.0%	-0.1%

List of Figures

1. Differences in the magnitude of the time-mean surface wind stress (N m^{-2}) between (a) CONTROL and NONE, (b) CONTROL and HEAT, and (c) HEAT and NONE. (d) differences in the mean wind stress curl (10^{-7} N m^{-3}) between CONTROL and NONE.
2. The time-mean surface heat flux (W m^{-2}) in (a) CONTROL and the differences between (b) CONTROL and NONE, (c) CONTROL and HEAT, and (d) HEAT and NONE.
3. As in Fig.2, but for the time-mean SST (°C).
4. The left column: differences in net surface heat flux (W m^{-2}) averaged over the first model day between (a) CONTROL and NONE, (b) CONTROL and HEAT, and (c) HEAT and NONE. The right column is the same as the left column, but for differences in SST (°C).
5. Differences in (a) wind power input to the ocean circulation (W m^{-2}) and its (b) ageostrophic component and (c) geostrophic component between CONTROL and NONE.
6. Wind power input to the ocean circulation (W m^{-2}) by the time-varying wind stress in (a) CONTROL and (b) the difference between CONTROL and NONE. (c) and (d) are for wind power input to surface geostrophic motions and (e) and (f) for wind power input to surface ageostrophic motions.
7. The left column: differences in the time-mean surface EKE (m^2 s^{-2}) between (a) CONTROL and NONE, (b) CONTROL and HEAT, and (c) HEAT and NONE.

The right column is the same as the left column, but for differences in the time-mean surface MKE ($m^2\ s^{-2}$).

8. The top row: EKE ($m^2\ s^{-2}$) averaged over (a) the global ocean, (b) the Southern Ocean, and (c) the tropical oceans in the three experiments. (d) is the percentage difference of the globally-averaged EKE between CONTROL and NONE. The bottom row is the same as the top row, but for the MKE.
9. As in Fig.2, but for the time-mean barotropic streamfuncions (Sv).
10. As in Fig.2, but for the March-mean MLD in the Northern Hemisphere and September-mean MLD in the Southern Hemisphere (m).
11. As in Fig.2, but for the time-mean AMOC (Sv).
12. The time-mean meridional heat transport (PW) of (a) the global ocean, (b) the Atlantic Ocean, (c) the Pacific Ocean, and (d) the Indian Ocean in CONTROL (green), HEAT (blue) and NONE (red).

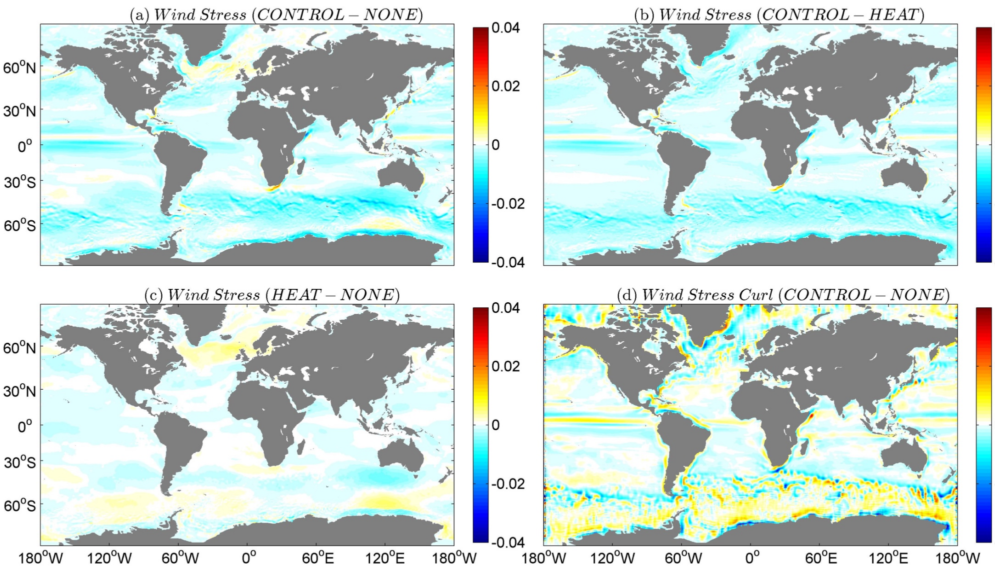

FIG. 1. Differences in the magnitude of the time-mean surface wind stress (N m^{-2}) between (a) CONTROL and NONE, (b) CONTROL and HEAT, and (c) HEAT and NONE. (d) differences in the mean wind stress curl (10^{-7} N m^{-3}) between CONTROL and NONE.

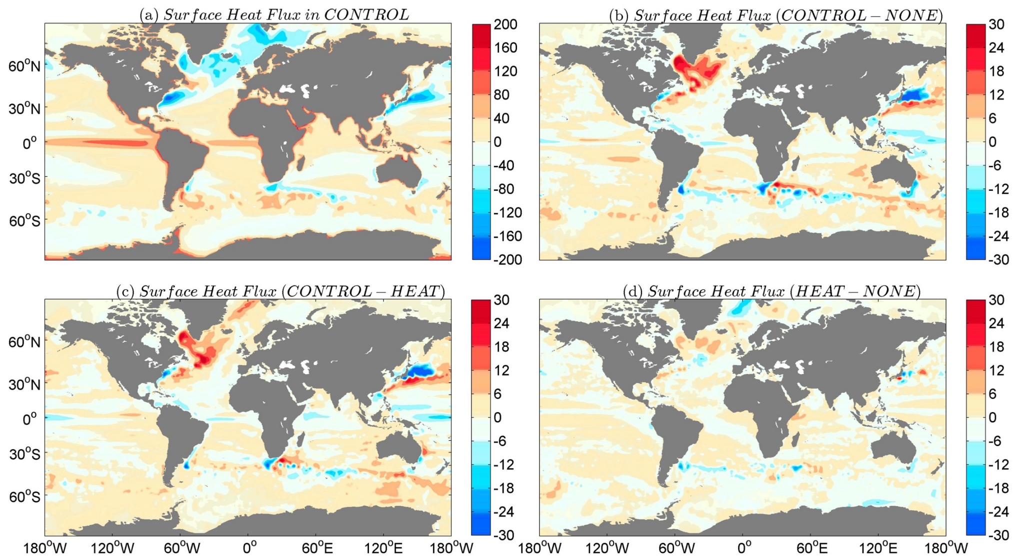

FIG. 2. The time-mean surface heat flux (W m^{-2}) in (a) CONTROL and the differences between (b) CONTROL and NONE, (c) CONTROL and HEAT, and (d) HEAT and NONE.

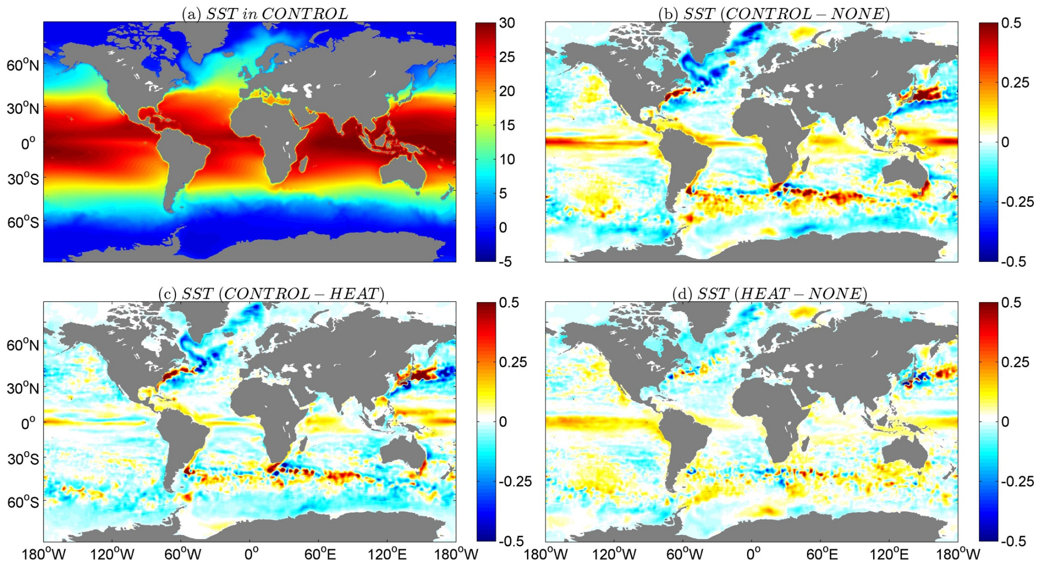

FIG. 3. As in Fig.2, but for the time-mean SST (°C).

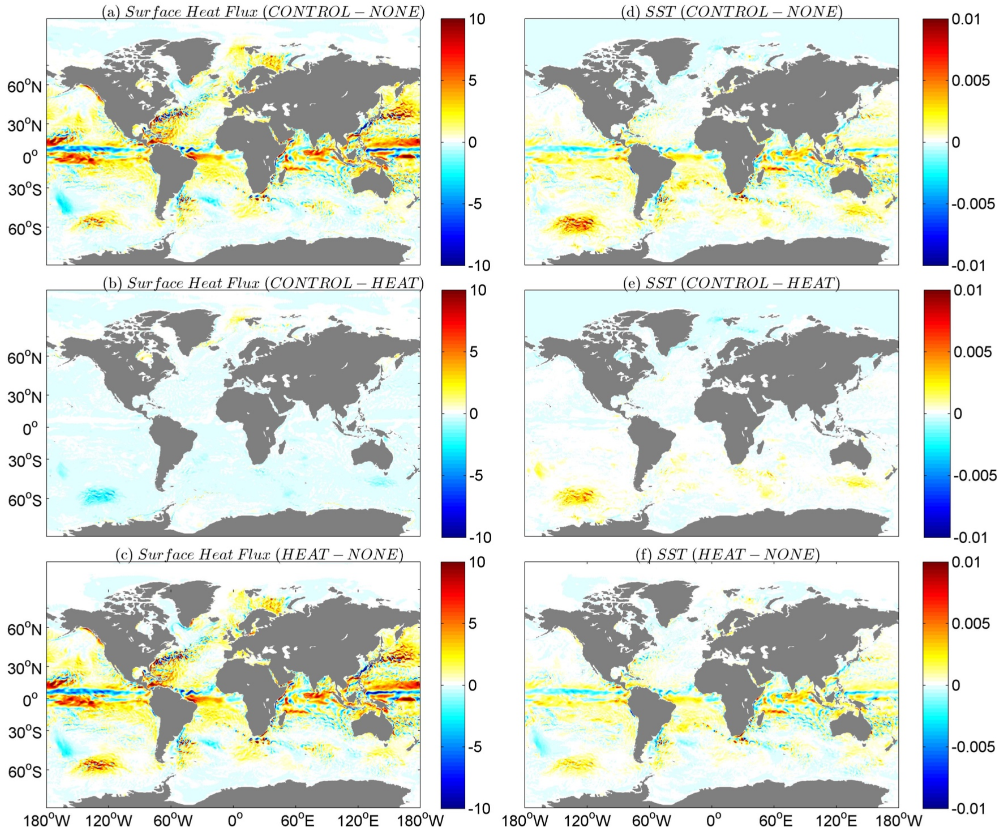

FIG. 4. The left column: differences in net surface heat flux (W m^{-2}) averaged over the first model day between (a) CONTROL and NONE, (b) CONTROL and HEAT, and (c) HEAT and NONE. The right column is the same as the left column, but for differences in SST (°C).

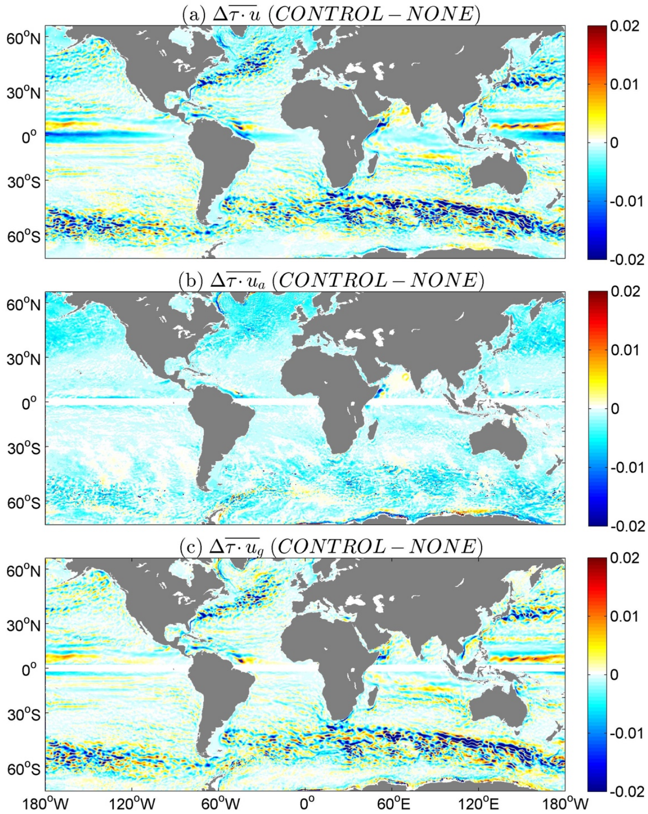

FIG. 5. Differences in (a) wind power input to the ocean circulation (W m^{-2}) and its (b) ageostrophic component and (c) geostrophic component between CONTROL and NONE.

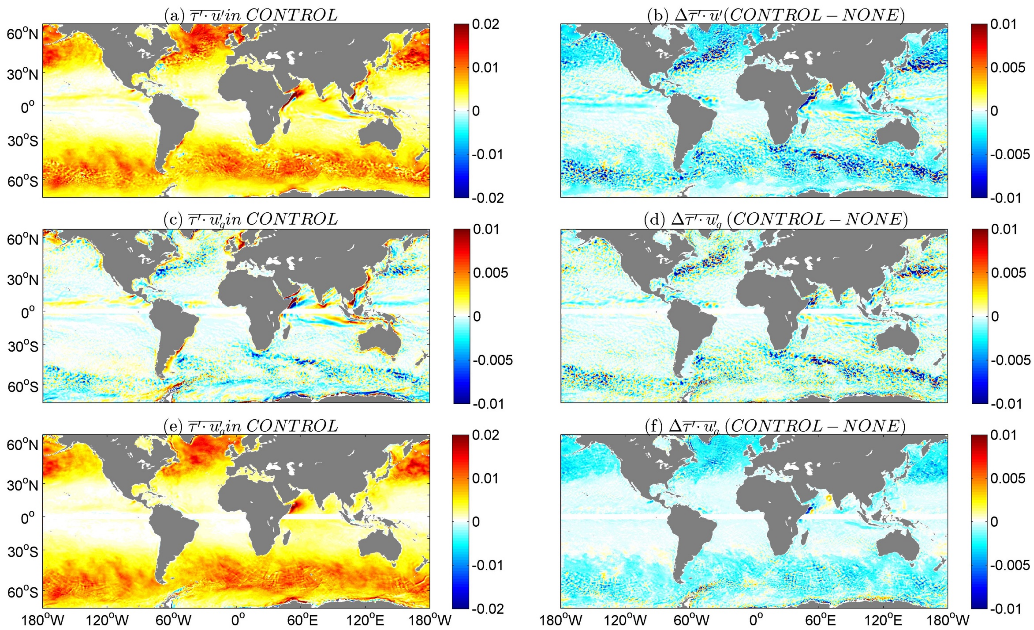

FIG. 6. Wind power input to the ocean circulation (W m^{-2}) by the time-varying wind stress in (a) CONTROL and (b) the difference between CONTROL and NONE. (c) and (d) are for wind power input to surface geostrophic motions and (e) and (f) for wind power input to surface ageostrophic motions.

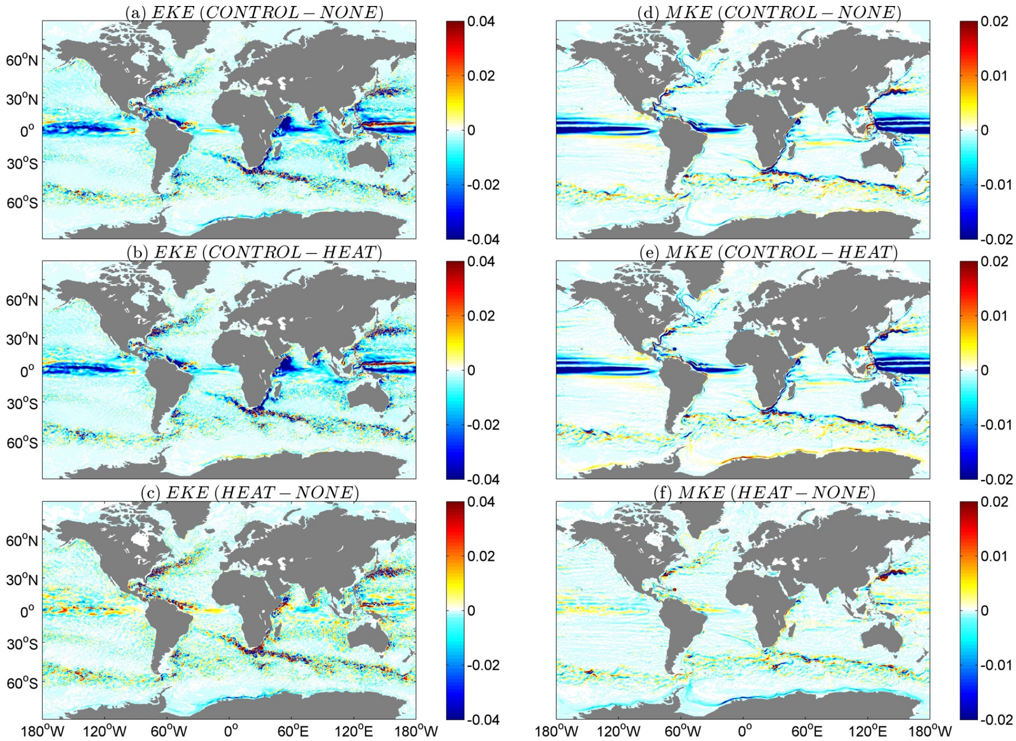

FIG. 7. The left column: differences in the time-mean surface EKE (m^2 s^{-2}) between (a) CONTROL and NONE, (b) CONTROL and HEAT, and (c) HEAT and NONE. The right column is the same as the left column, but for differences in the time-mean surface MKE (m^2 s^{-2}).

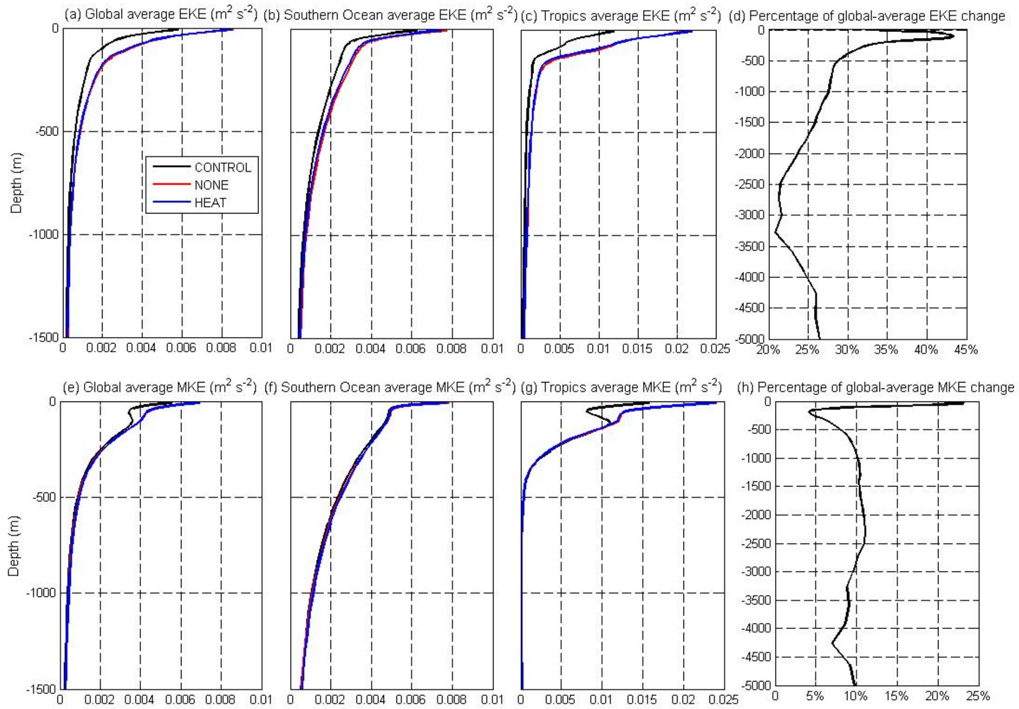

FIG. 8. The top row: EKE (m^2 s^{-2}) averaged over (a) the global ocean, (b) the Southern Ocean, and (c) the tropical oceans in the three experiments. (d) is the percentage difference of the globally-averaged EKE between CONTROL and NONE. The bottom row is the same as the top row, but for the MKE.

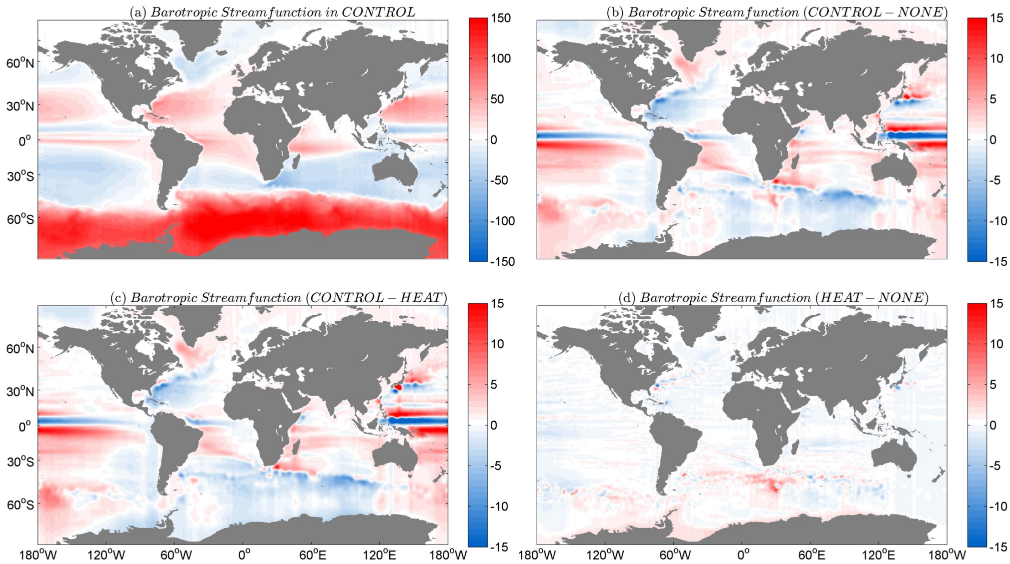

FIG. 9. As in Fig.2, but for the time-mean barotropic streamfuncions (Sv).

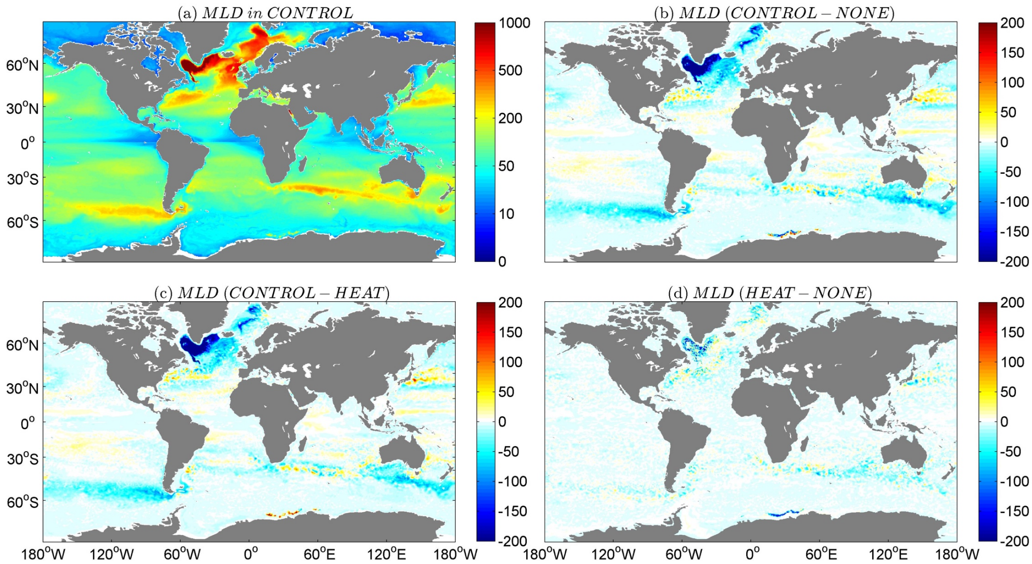

FIG. 10. As in Fig.2, but for the March-mean MLD in the Northern Hemisphere and September-mean MLD in the Southern Hemisphere (m).

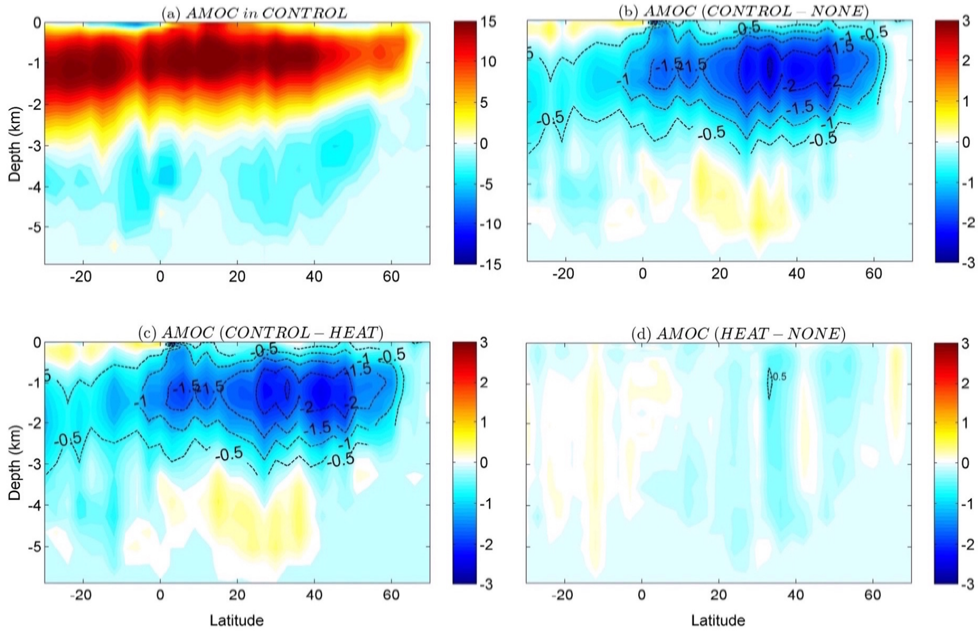

FIG. 11. As in Fig.2, but for the time-mean AMOC (Sv).

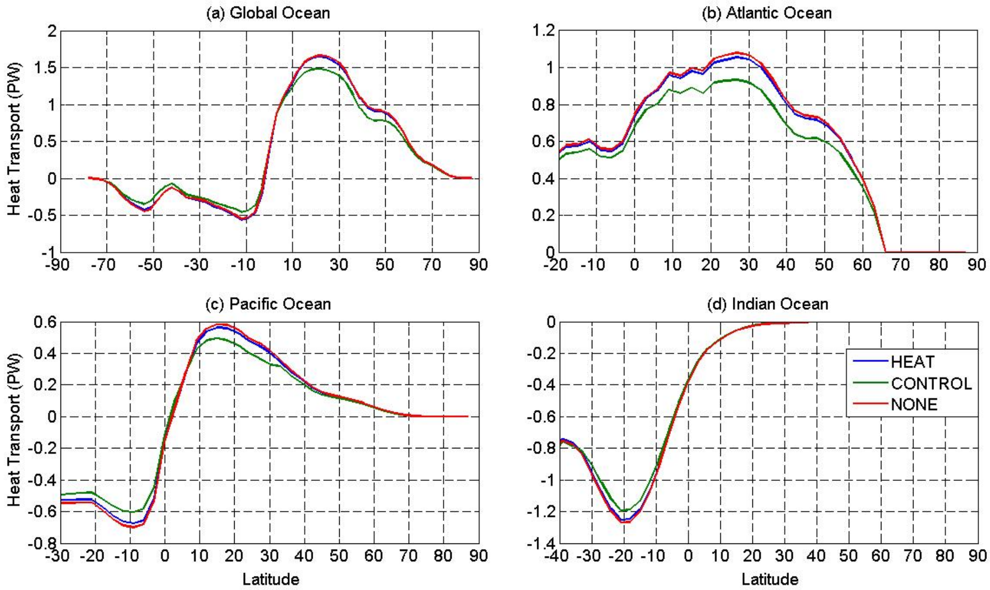

FIG. 12. The time-mean meridional heat transport (PW) of (a) the global ocean, (b) the Atlantic Ocean, (c) the Pacific Ocean, and (d) the Indian Ocean in CONTROL (green), HEAT (blue) and NONE (red).